BIOCHEMISTRY
including biophysical chemistry & molecular biology

Article

pubs.acs.org/biochemistry

Multivalent Display of Antifreeze Proteins by Fusion to Self-Assembling Protein Cages Enhances Ice-Binding Activities

Sean W. Phippen,[†] Corey A. Stevens,[†] Tyler D. R. Vance,[†] Neil P. King,[‡,§] David Baker,[‡,§,∥] and Peter L. Davies*[,†]

[†]Department of Biomedical and Molecular Sciences, Queen's University, Kingston, Ontario K7L 3N6, Canada
[‡]Department of Biochemistry, University of Washington, Seattle, Washington 98195, United States
[§]Institute for Protein Design, University of Washington, Seattle, Washington 98195, United States
[∥]Howard Hughes Medical Institute, University of Washington, Seattle, Washington 98195, United States

Supporting Information

ABSTRACT: Antifreeze proteins (AFPs) are small monomeric proteins that adsorb to the surface of ice to inhibit ice crystal growth and impart freeze resistance to the organisms producing them. Previously, monomeric AFPs have been conjugated to the termini of branched polymers to increase their activity through the simultaneous binding of more than one AFP to ice. Here, we describe a superior approach to increasing AFP activity through oligomerization that eliminates the need for conjugation reactions with varying levels of efficiency. A moderately active AFP from a fish and a hyperactive AFP from an Antarctic bacterium were genetically fused to the C-termini of one component of the 24-subunit protein cage T33-21, resulting in protein nanoparticles that multivalently display exactly 12 AFPs. The resulting nanoparticles exhibited freezing point depression >50-fold greater than that seen with the same concentration of monomeric AFP and a similar increase in the level of ice-recrystallization inhibition. These results support the anchored clathrate mechanism of binding of AFP to ice. The enhanced freezing point depression could be due to the difficulty of overgrowing a larger AFP on the ice surface and the improved ice-recrystallization inhibition to the ability of the nanoparticle to simultaneously bind multiple ice grains. Oligomerization of these proteins using self-assembling protein cages will be useful in a variety of biotechnology and cryobiology applications.

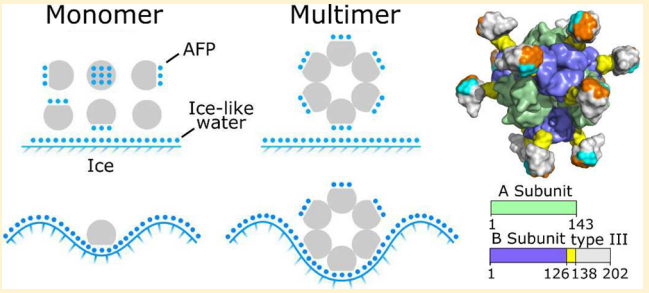

Ice-binding proteins (IBPs) are typically small (3−30 kDa) single-domain proteins capable of adsorbing to the surface of ice.[1,2] IBPs were first found in fish and arthropods, where they are able to inhibit ice crystal growth and convey freeze resistance to the organism. These IBPs are commonly known as antifreeze proteins (AFPs). Other IBPs convey freeze tolerance to organisms, such as plants, which allows them to survive the formation of ice in their tissues by inhibiting ice recrystallization.[3]

IBPs exhibit a variety of folds, an observation that has been attributed to their recent independent evolution in multiple species.[1,2,4] However, despite these differences in overall structure, IBPs have in common a flat, relatively hydrophobic face, which acts as the ice-binding site (IBS) of the protein. The IBS has been predicted[5,6] and shown[7] to orient water molecules into an ice-like lattice, which merges with the quasi-liquid layer on ice that then freezes the IBP onto its surface. This freezing adsorption of IBPs to ice causes a microcurvature of the crystal surface, making it thermodynamically more difficult for water molecules to add to the crystal.[8,9] This binding and altering of the ice crystal surface result in a depression of the freezing point of the ice-containing solution, as well as a slight increase in melting point, a phenomenon termed thermal hysteresis (TH).[1,2]

IBPs are increasingly being used in biotechnology and cryobiology.[10−12] For all of these applications, increasing the activity of IBPs would be beneficial from a cost perspective. Similar levels of TH and ice-recrystallization inhibition could be achieved with lower concentrations of IBP. Also, the temperature to which materials might be cooled without freezing could be lowered.

Several factors increase IBP activity.[13] Both TH and ice-recrystallization inhibition activity increase with an increase in IBP concentration, even though adsorption of IBP to ice is irreversible.[9,14,15] This occurs in part because ice binding by IBPs is a diffusion-controlled reaction, with the rate-limiting step being the IBP coming into contact with the ice and making a productive bonding interaction. For the latter to occur, there should be sufficient ice-like waters on the IBS of the IBP to merge with and freeze to the quasi-liquid layer around ice. To

Received: August 26, 2016
Revised: November 9, 2016
Published: November 11, 2016

DOI: 10.1021/acs.biochem.6b00864
Biochemistry 2016, 55, 6811−6820

increase the number of ice-like waters, two strategies have been employed. One is to increase the surface area of the IBS; the other is to link together a number of IBSs that can simultaneously bind ice. In nature, the former strategy manifests in natural isoforms that have additional sequence repeats that expand the surface area of the IBS.[16−19] This strategy has been mimicked for a β-solenoid AFP by increasing the number of helical coils.[20]

The second strategy, of having more than one IBS, also occurs in nature with a natural dimer of type III AFP from the Antarctic eel pout (*Rhigophila dearborni*).[21] Nishimiya et al. assessed the activity of linear multimers of the type III AFP by recombinantly linking monomers and dimers to form a chain up to four AFPs long.[22] These authors noted that an increase in thermal hysteresis activity was apparent on both a molar basis and a per domain basis. To help tease out the contributions of size and number of ice-binding sites to TH activity, a recombinant type III AFP dimer was synthesized from a duplicated monomer.[23] The dimer was twice as active as the monomer, whereas genetically fusing the AFP to one that is inactive or facing the opposite direction resulted in an only 1.2-fold increase in activity. In another example of this strategy, a recombinant form of the single α-helix type I AFP was conjugated via its C-terminal end to the primary amines of polyallylamine chains.[24] The effects of AFP multimeric conjugation have also been investigated by conjugating the globular 7 kDa HPLC12 isoform of type III AFP from the ocean pout (*Macrozoarces americanus*) through a C-terminal cysteine residue to a second-generation polyamidoamine (PAMAM) dendrimer using a heterobifunctional cross-linker.[25] AFPs that were conjugated to polyallylamine chains and PAMAM dendrimers exhibited 2- and >4-fold increases in TH activity, respectively, compared to that of the monomeric AFP. AFPs bound to PAMAM dendrimers also exhibited 8−10-fold stronger ice-recrystallization inhibition.

Conjugating AFPs to branched molecules such as polyamidoamine or polyallylamine involved chemical reactions with varying degrees of efficiency, which affected the number of AFPs actually incorporated into the structures. The number of type I AFPs attached to polyallylamine was not quantified,[24] while mass spectrometry revealed that 6−11 AFPs of a maximum of 16 were connected to the PAMAM dendrimers.[25] To overcome this limitation and present more AFPs together as one unit, we genetically fused them to the termini of self-assembling protein subunits that form oligomers. Using this strategy, AFPs are connected to the oligomers in a defined stoichiometry during biosynthesis, ensuring maximal occupancy of AFPs on the termini of the self-assembling subunits.

Protein self-assembly is employed by many proteins in nature for specific structural or functional purposes.[26−28] Existing protein assemblies have been altered in the past by genetically fusing additional domains in a manner that decorates their surface, generating multimers out of normally monomeric proteins.[29] However, it has been reasoned that novel assemblies must be generated to have protein multimers that suit the functional needs of specific biotechnology applications.[30]

Designing novel protein assemblies has been a long-standing goal in biotechnology.[31] In a pioneering study 15 years ago, the subunits of two existing oligomers were genetically fused to generate a 12-subunit protein cage with tetrahedral point group symmetry.[32] With increases in computing power and the development of new design methods, substantial progress has recently been made in the computational design of novel protein assemblies. Using the RosettaDesign software,[33] it has been possible to design novel interaction interfaces between existing oligomers to generate a variety of protein assemblies such as one-component[34] and two-component[35] nanoparticles and two-dimensional protein arrays.[36]

Here, we describe the development of a set of fusion proteins that incorporate AFPs onto the surface of the designed assembly T33-21, a 24-subunit protein cage with tetrahedral symmetry.[35] This structure contains two types of subunits, designated T33-21A and T33-21B, each of which form four homotrimers within the assembly (Figure 1A). The developed

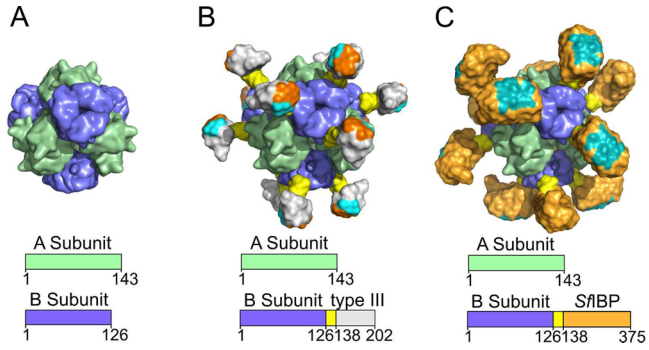

Figure 1. Design of self-assembling AFP multimers. (A) Surface representation of the design model for the self-assembling protein cage T33-21 consisting of four T33-21A trimers (light green) and four T33-21B trimers (violet), with like trimers arranged with tetrahedral point group symmetry. (B) Model of the type III AFP multimer, which consists of T33-21 with type III AFP (gray) decorating the surface. The compound ice-binding site of type III AFP is also shown, with the pyramidal plane-binding segment colored orange and the primary prism plane segment cyan. Each AFP is attached to the C-terminus of a T33-21B subunit by a helical linker (yellow). (C) Model of the *Sf*IBP multimer, which consists of T33-21 decorated on the surface with 12 *Sf*IBPs (orange). The putative ice-binding site of the AFP is also shown (colored teal). Included below each model are diagrams representing the domain architecture of both subunits A and B of T33-21, as well as the AFPs genetically fused to subunit B. Residue numbers are indicated below the bars.

fusion proteins consist of the T33-21B subunit connected via a helical linker to one of two AFPs. First, T33-21B was fused to the moderately active type III AFP expressed in the ocean pout *M. americanus* (Figure 1B).[37] Separately, it was also fused to *Sf*IBP, a hyperactive AFP secreted by the Antarctic bacterium *Shewanella frigidimarina* (Figure 1C).

MATERIALS AND METHODS

Design of the AFP-Containing T33-21 Multimers. The models of four two-component protein cages (T32-28, T33-15, T33-21, and T33-29)[35] were examined in PyMOL[37] to find a design containing outward-facing C-termini that could be easily targeted for the genetic fusion of an AFP. Protein cage T33-21 was chosen to present the AFPs on its surface, as subunit B of this design has such an outward-facing C-terminus and the pET-29b expression vector encoding this design contains a single *Xho*I site immediately downstream of the gene for this subunit. Genes encoding subunits A and B of T33-21 are found on the same pET-29b vector and are flanked by upstream *Nde*I sites, while only the gene encoding the T33-21B subunit is flanked by a downstream *Xho*I site (Figure S1A). To join AFPs to the C-terminus of the T33-21B subunit, synthetic genes encoding the AFPs (GeneArt) were flanked on both sides by

DOI: 10.1021/acs.biochem.6b00864
Biochemistry 2016, 55, 6811−6820

*Xho*I sites (Figure S1B). One gene encoded the sequence of the fully active HPLC12 isoform of type III AFP from *M. americanus* [Protein Data Bank (PDB) entry 1HG7], which has the C-terminal residues YPPA replaced by YAA.[39] The other gene contained the sequence for *Sf*IBP from *S. frigidimarina* (GenBank entry LRDC00000000). Each gene also encoded an N-terminal helical linker with the sequence AEAAAKEAAAKA, to extend the AFP away from the C-terminus of the T33-21B subunit and reduce the likelihood of steric interference with self-assembly. A model of the type III multimer (Figure 1) was generated in PyMOL[38] using the design model for T33-21[35] and the crystal structure of type III AFP.[40] A model of the *Sf*IBP multimer was made in a similar fashion, using the design model for T33-21 and a model for *Sf*IBP generated using the Phyre2 server.[41]

Cloning. AFP-encoding genes were ligated into the two-component pET-29b expression vector encoding the T33-21 subunits. Briefly, 1 μg of the vector was digested with *Xho*I and then with shrimp alkaline phosphatase (SAP). The cut and dephosphorylated vector was combined with the AFP gene insert in a 3:1 molar ratio and ligated using T4 DNA ligase. The ligated DNA was transformed into DH5α competent cells and plated on agar plates containing kanamycin (100 μg/mL). The purified expression vector from positive clones was digested with a restriction endonuclease (*Ase*I for the type III-containing construct, *Apo*I for the *Sf*IBP-containing construct) to check the orientation of the insert, and vectors displaying the appropriate banding pattern on an agarose gel were sent for authentication by sequencing.

Expression and Purification. Both AFP-containing constructs were expressed in *Escherichia coli* BL21 (DE3) cells as described previously.[42] Briefly, BL21 cells containing the appropriate expression vector were added to Luria-Bertani broth containing kanamycin (100 μg/mL) and incubated at 37 °C until an OD_{600} of 0.5 was reached. The BL21 cells were then incubated at 23 °C until the OD_{600} increased to 1.0. At this point, the culture was induced with 1 mM isopropyl β-D-1-thiogalactopyranoside and incubated at 23 °C overnight. Constructs were also purified as described previously,[25] which included the centrifugation of induced BL21 cells at 4000 rpm for 30 min using a Beckman Coulter JS 4.2 rotor. Pelleted cells were resuspended in a lysis buffer containing 50 mM Tris-HCl (pH 8.0), 250 mM NaCl, 5 mM imidazole, 1 mM phenylmethanesulfonyl fluoride (PMSF), and 10 mM β-mercaptoethanol and lysed by sonication using a Fisher Scientific Sonic Dismembrator (model 5000). Bacterial lysates were centrifuged at 16000 rpm for 30 min using a Beckman Coulter JA 25.5 rotor, and the AFP-decorated cages were recovered from the lysate supernatant by Ni^{2+}-nitrilotriacetate chromatography. The eluate totalling approximately 20 mL was concentrated using centrifugal filters with a molecular weight cutoff of 10 kDa to a volume of approximately 5 mL, and the cages were further purified using a HiLoad 16/60 Superdex 200 prep grade size-exclusion column (Amersham), which was equilibrated with a running buffer containing 25 mM Tris-HCl (pH 8.0), 150 mM NaCl, and 10 mM β-mercaptoethanol. Fractions containing the assembled AFP multimers were pooled and concentrated using centrifugal filters. Protein concentrations were measured by absorbance at 280 nm using molar extinction coefficients calculated from the protein parameters using the ExPASy ProtParam online tool.

Ice Crystal Morphology and Thermal Hysteresis Measurements. TH of the assembled structures was measured as previously described.[43,25] Briefly, samples were suspended in oil droplets and cooled on a Clifton nanoliter stage using a model 3040 temperature controller (Newport). The temperature was decreased below the melting point by 0.01 °C every 0.4 s for the *Sf*IBP-containing constructs and by 0.005 °C every 0.4 s for the type III-containing constructs and the negative controls. Protein samples were dissolved in 25 mM Tris-HCl (pH 8.0), 150 mM NaCl, and 10 mM β-mercaptoethanol. Ice crystal images and videos were captured using a Panasonic WV-BL200 digital camera, with videos recorded at a rate of 30 frames/s.

Ice-Recrystallization Inhibition Assays. Ice-recrystallization inhibition assays were performed on the AFP-containing assemblies and T33-21 by the "splat" method as previously described.[25] Protein samples were dissolved in 25 mM Tris-HCl (pH 8.0), 150 mM NaCl, 0.01 mg/mL bovine serum albumin, and 10 mM β-mercaptoethanol. Images of "splats" (ice wafers) were captured using a Nikon D3000 camera after incubation in 2,2,4-trimethylpentane at −6 °C for 18 h.

FIPA Analysis. FIPA (fluorescence-based ice plane affinity) analysis was conducted as described by Basu et al.[44] Briefly, 3 mg of protein in Tris-HCl buffer was exchanged into 1 mL of 50 mM HEPES (pH 8.5), 150 mM NaCl, and 10 mM β-mercaptoethanol and labeled with 6-[fluorescein-5(6)-carboxamido] hexanoic acid (0.3 mg). The labeled protein was separated from the free label using a Sephadex G-25 M desalting column. The labeled protein was then added to 25−30 mL of a cooled (4 °C) buffer containing 25 mM Tris-HCl (pH 8.0), 150 mM NaCl, and 10 mM β-mercaptoethanol, with an ice hemisphere mounted on a coldfinger cooled to −5 °C immersed in the solution. For the 6-[fluorescein-5(6)-carboxamido] hexanoic acid negative control (Figure 5E), 0.3 mg of the label was added directly to this solution. The ice hemisphere was submerged and grown in the buffer for 2−3 h and then photographed at 4 °C under 470 nm illumination using a Nikon D3000 camera with a 515 nm emission filter. The ice binding pattern of AFP multimers was compared to those of their corresponding monomeric AFPs (Table S1), the *Sf*IBP monomer, and nfeAFP8, a fully active QAE1 isoform of type III AFP expressed in the Japanese eelpout *Zoarces elongatus*.[44]

RESULTS

AFP Multimers Self-Assemble. To generate AFP multimers using the subunits of the self-assembling protein cage T33-21 (Figure 1), synthetic genes encoding both the moderately active type III AFP from *M. americanus* and the hyperactive *Sf*IBP from *S. frigidimarina* were cloned into the expression vector encoding T33-21. This strategy connected AFPs via their N-termini to the C-termini of the protein cage B subunits by a 12-residue helical linker to decorate the surface of the assembly with 12 AFPs. Both AFP-containing designs were successfully expressed in *E. coli*. After nickel affinity chromatography, the AFP-decorated cages were purified to homogeneity by size-exclusion chromatography. The two AFP multimers generated elution profiles that were distinct from that of T33-21 alone (Figure 2). T33-21 (391 kDa) elutes from the Superdex 200 column as one major peak, with an elution volume of 69.3 mL (Figure 2A). This assembly elutes just after ferritin (elution volume of 67.1 mL), a protein standard with a slightly higher molecular weight (440 kDa). In contrast, three peaks were observed during elution of the type III AFP multimer from the size-exclusion column (Figure 2B). The first

DOI: 10.1021/acs.biochem.6b00864
Biochemistry 2016, 55, 6811−6820

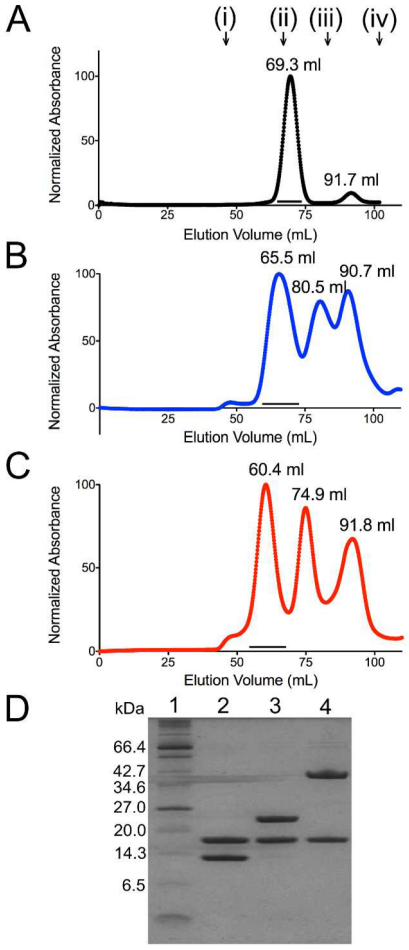

Figure 2. SDS–PAGE and size-exclusion chromatography of AFP multimers. Superdex 200 size-exclusion elution profiles were generated for (A) T33-21, (B) the type III AFP multimer, and (C) the *Sf*IBP multimer. Black arrows represent the elution volumes of protein standards (i) blue dextran (2000 kDa, 46.3 mL), (ii) ferritin (400 kDa, 67.1 mL), (iii) albumin (67 kDa, 83.3 mL), and (iv) ribonuclease (13.7 kDa, 101.9 mL). Black bars represent fractions pooled and concentrated for additional experiments. (D) SDS–PAGE analysis of 5 μg samples of T33-21 and the AFP multimers: lane 1, molecular weight markers; lane 2, T33-21; lane 3, type III AFP multimer; lane 4, *Sf*IBP multimer.

peak eluted earlier (65.5 mL) than T33-21 and the ferritin standard with an apparent molecular weight of 502 kDa. Sodium dodecyl sulfate–polyacrylamide gel electrophoresis (SDS–PAGE) revealed that this peak contains the same A subunit (19.3 kDa) as the T33-21 control and that the B subunit (14.3 kDa) has shifted from an apparent molecular weight of 14.3 to 22.5 kDa, consistent with the addition of an 8.2 kDa domain (Table 1). The staining intensity of the two constituent bands is consistent with a 1:1 stoichiometry (Figure 2D). These findings led to the conclusion that the largest peak in the Figure 2B profile contains the assembled type III multimer with a calculated molecular weight of 502 kDa compared to an apparent molecular weight of 502 kDa (Table 2).

Elution of the *Sf*IBP multimer from the Superdex 200 column also revealed three distinct peaks (Figure 2C). As was observed for the type III multimer, only the first peak at 60.4 mL (apparent molecular weight of 710 kDa) eluted earlier than that of T33-21 and that of the type III AFP-decorated cage. It

Table 1. Observed Molecular Weights of T33-21 and AFP Multimer Subunits Predicted Using SDS–PAGE

design	subunit	expected MW (kDa)	observed MW (kDa)	percent error (%)
T33-21	A	19.3	15.3	21
	B	14.3	11.5	19
type III T33-21	A	19.3	15.3	21
	B	22.5	20.7	8
*Sf*IBP T33-21	A	19.3	15.3	21
	B	39.9	41.9	5

Table 2. Observed Molecular Weights of Assembled AFP Multimers Predicted Using Size-Exclusion Chromatography

design	expected MW (kDa)	observed MW (kDa)	percent error (%)
T33-21	391	342	13
type III multimer	502	502	0
*Sf*IBP multimer	710	841	18

contained both subunits necessary to form the multimer with the A subunit unchanged and the B subunit shifted from an apparent molecular weight of 14.3 to 39.9 kDa, consistent with the addition of a 25.6 kDa domain. The assembled *Sf*IBP multimer was calculated to have a molecular weight of 841 kDa, compared to the apparent molecular weight of 710 kDa. Fractions containing the assembled AFP multimers were pooled, as indicated by the bars under the peaks in panels B and C of Figure 2 and concentrated for use in subsequent experiments.

AFP Multimers Have Enhanced Antifreeze Activity. The activity of AFPs connected by a scaffold can be evaluated in two ways: either on the basis of the concentration of the AFP multimer as a unit or on the basis of the concentration of the AFP domains as if they were free in solution.[25] The TH activities of the type III AFP and *Sf*IBP multimers were compared to those of both the monomeric AFPs and T33-21 (Figure 3). T33-21 had no ability to depress the freezing point of the solution ($\bar{x}$ = 0.01 °C; n = 3), with TH values indistinguishable from that of the S200 running buffer negative control ($\bar{x}$ = 0.01 °C; n = 3). The TH activity for 25 μM monomeric type III AFP (Figure 3A) was interpolated from an activity curve for the wild-type form of the protein,[45] to give a value of 0.1 °C. A 2.1 μM solution of the type III AFP multimer is equivalent to a 25 μM solution of the AFP-containing B subunit if the multimers were to completely dissociate. Its TH activity ($\bar{x}$ = 0.33 °C; n = 3) at this concentration (2.1 μM) was 3 times larger than the value for 25 μM monomeric type III AFP. TH values for the monomeric *Sf*IBP were also previously measured as a function of protein concentration, and the activity at 25 μM was interpolated from the existing data to be 1.25 °C. The *Sf*IBP multimer at 2.1 μM is equivalent to 25 μM *Sf*IBP-containing B subunit and exhibited 2.5-fold greater TH activity ($\bar{x}$ = 3.15 °C; n = 6) compared to that of monomeric *Sf*IBP at the same molar concentration.

When TH activities were compared on the basis of the multimer concentration of 2.1 μM, the monomeric type III AFP at this concentration had a TH value that was barely detectable ($\bar{x}$ = 0.02 °C; n = 3). The TH activity of monomeric *Sf*IBP at a concentration of 2.1 μM ($\bar{x}$ = 0.12 °C; n = 3)

DOI: 10.1021/acs.biochem.6b00864
Biochemistry 2016, 55, 6811–6820

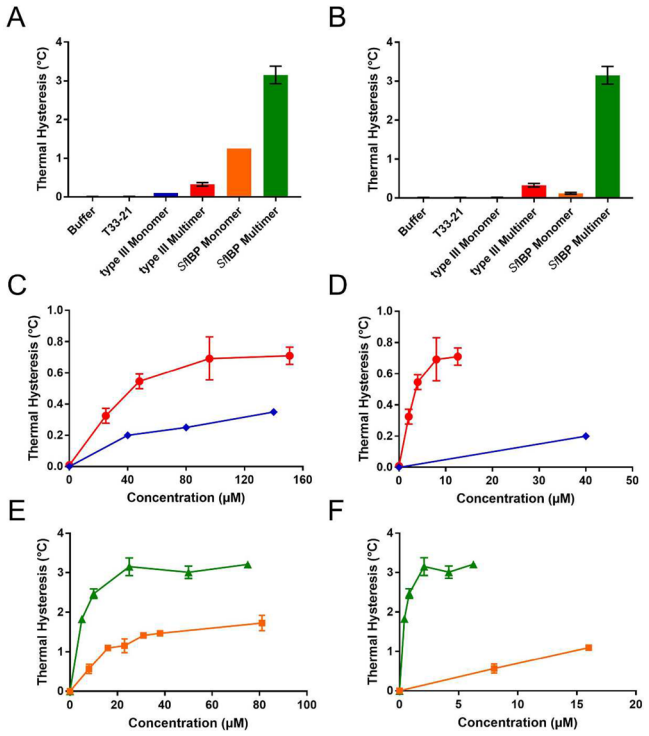

Figure 3. Thermal hysteresis activity of AFP multimers and monomeric AFPs. (A) TH activity was compared on a "per-AFP" basis by measuring the activity for solutions containing 25 μM AFP-containing B subunit of the AFP multimers and T33-21, and the same concentration of the monomeric AFPs. (B) TH activity was also compared on a "per-particle" molar basis by calculating the concentration of the assembled AFP multimer, which has a 1:12 stoichiometry compared to the B subunit. TH measurements of AFP multimers and monomeric AFPs were taken at a concentration of 2.1 μM. The TH activities exhibited by the type III multimer (red circles) and monomeric type III AFP (blue diamonds) were further compared across a range of concentrations on (C) a "per-AFP" basis and (D) a "per-particle" basis. Finally, the TH activities of the *Sf*IBP multimer (green triangles) and monomer (orange squares) were compared across a range of concentrations on (E) a "per-AFP" basis and (F) a "per-particle" basis. Error bars indicate the standard deviation of the mean for each TH measurement.

exhibited 26-fold less activity than the *Sf*IBP multimer (Figure 3B).

To examine the concentration dependence of the enhanced TH activity observed for AFP multimers, we measured activity for the type III multimer across a concentration range of 0−150 μM of the AFP-containing B subunit (Figure 3C). The activity curve of the type III multimer resembled a rectangular hyperbola, approaching a plateau around 0.7 °C at concentrations of >100 μM. When compared on a "per-AFP" basis, the activity of the type III multimer was at least 2-fold greater than that of the monomer across all concentrations. When compared on a "per-particle" basis (Figure 3D), the difference is much more striking; over the particle concentration range of 0−13 μM, the activity of the type III multimer was at least 10-fold greater than that of the monomer, with the greatest increase (25-fold) occurring at 4 μM.

The *Sf*IBP multimer exhibited even more potent TH activity. Its curve also resembled a rectangular hyperbola approaching a plateau around 3.1 °C at B subunit concentrations of >25 μM. When compared to the monomer on a "per-AFP" basis (Figure 3E), the *Sf*IBP multimer showed activity at least 2-fold greater than that of the monomer across a concentration range of 0−75 μM. When compared on a "per-particle" basis (Figure 3F), the multimer exhibited an at least 7-fold increase in TH activity across the concentration range of 0−6.25 μM, with the greatest increase (>50-fold) occurring at 5 μM, the lowest concentration measured.

Multimerization of Type III AFP Alters the Ice Crystal "Burst" Pattern. Single ice crystals formed and observed in solutions containing T33-21 and the AFP multimers during TH measurements provide important clues about the activity of the engineered antifreeze constructs, as do the "burst" patterns of ice crystals bound by the AFP multimers when the AFP-depressed freezing points are surpassed (Figure 4). No faceting

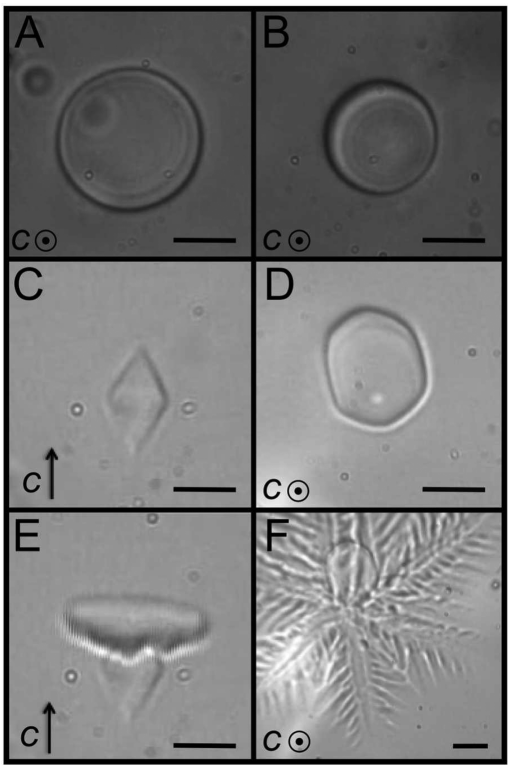

Figure 4. Ice crystal shaping and burst patterns. Ice crystal shaping was observed during TH measurements for (A) Superdex 200 running buffer, (B) 2.1 μM T33-21, (C) 2.1 μM type III AFP multimer, and (D) 1.6 μM *Sf*IBP multimer. Ice crystal bursts below the AFP-depressed freezing point were also observed for crystals bound by (E) the type III AFP multimer (2.1 μM) and (F) the *Sf*IBP multimer (1.6 μM). The direction of the *c*-axis of the ice crystal is indicated by the black arrows. The black scale bars represent a distance of 10 μm.

was observed on ice crystals immersed in the Superdex 200 running buffer (Figure 4A) or in the solution containing T33-21 (Figure 4B). Instead, ice crystals exhibited the standard disklike morphology normally observed in solutions lacking AFPs.

The type III multimer shaped ice crystals into hexagonal bipyramids, with the *c*-axis of the ice crystal passing through the two apices (Figure 4C). This is the same morphology observed for ice crystals bound by monomeric type III AFP.[46,47] The *Sf*IBP multimer shaped ice into crystals with a hexagonal morphology (Figure 4D) similar to that observed previously for certain hyperactive AFPs.[46]

Once the freezing point was surpassed, ice crystals bound by the type III AFP and *Sf*IBP multimers "burst" normal to the *c*-

DOI: 10.1021/acs.biochem.6b00864
Biochemistry 2016, 55, 6811−6820

axis of the crystal (panels E and F of Figure 4, respectively). Ice crystal growth perpendicular to the *c*-axis is characteristic of hyperactive AFPs that bind the basal plane of ice in addition to prism and/or pyramidal planes, and the fractal burst pattern is commonly seen with these more active AFPs as a result of greater supercooling of the AFP-containing solution. However, ice crystals bound by type III AFPs normally burst parallel to the *c*-axis when the freezing point is reached.[46] To investigate the basis for this change in behavior, we set out to determine the planes of ice to which the AFP multimers bound.

The Ice Binding Pattern of Type III AFP Is Altered by Multimerization. To determine if the oligomerization of type III AFP and *Sf*IBP altered their binding to ice, the AFP multimers were fluorescently labeled and studied using FIPA analysis (Figure 5). The type III AFP QAE1 isoform used for these experiments binds to both the primary prism and a pyramidal plane of ice.[48] These planes of ice are sited on the perimeter of the ice hemisphere when the *c*-axis of the ice crystal is perpendicular to the plane of the page. The binding of nfeAFP8, also a fully active QAE1 isoform of type III AFP, to these planes after labeling with Pacific Blue results in fluorescence along the perimeter of the ice hemisphere and none on the basal plane of the crystal (Figure 5A).[44] When the type III multimer was labeled and incubated with the crystal hemisphere, there was binding to the primary prism planes and not to the basal plane, which was expected (Figure 5B). However, the labeled type III multimer did not appear to bind well to the pyramidal planes of ice in comparison to the pattern produced by monomeric type III AFP (Figure 5A), which is why the fluorescent illumination in Figure 5B is confined to the equator of the hemisphere.

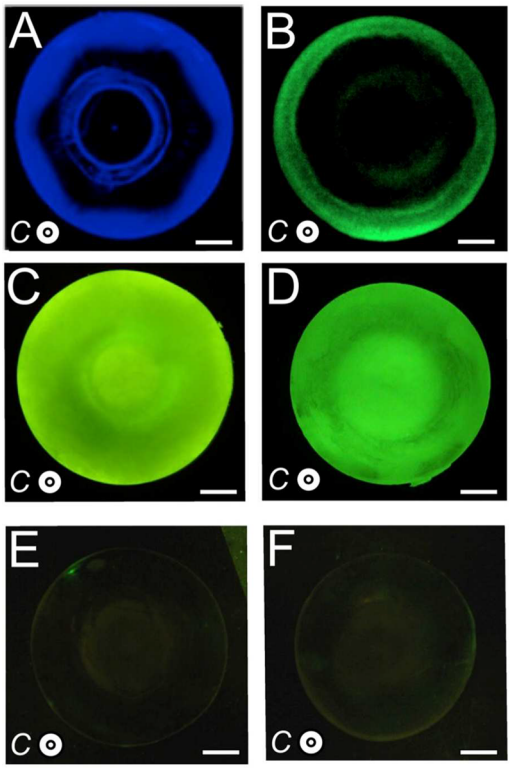

Figure 5. Ice plane affinity of AFP multimers and monomeric AFPs. FIPA results are shown for (A) monomeric type III AFP, (B) the type III multimer, (C) monomeric *Sf*IBP, (D) the *Sf*IBP multimer, (E) the 6-[fluorescein-5(6)-carboxamido] hexanoic acid negative control, and (F) the T33-21 negative control. All protein samples were labeled with 6-[fluorescein-5(6)-carboxamido] hexanoic acid except for monomeric type III AFP, which was labeled with Pacific Blue dye. The white scale bars represent a distance of 1 cm. In each result, the *c*-axis runs perpendicular to the plane of the image.

Monomeric *Sf*IBP bound to the entire ice hemisphere during FIPA analysis (Figure 5C), due to the ability of this hyperactive AFP to bind to the basal plane of ice as well as prism and pyramidal planes. We observed the same promiscuous binding with the *Sf*IBP multimer (Figure 5D), indicating that multimerization did not qualitatively change the ability of this AFP to bind these multiple planes of ice.

T33-21 was also labeled and subject to FIPA analysis, during which we observed only background levels of fluorescence on the ice hemisphere (Figure 5F), similar to the case for the 6-[fluorescein-5(6)-carboxamido] hexanoic acid negative control (Figure 5E). We conclude that T33-21 is unable to bind to ice without the addition AFPs to its surface, which is consistent with the lack of TH activity measured with the undecorated cage.

AFP Multimers Exhibit Enhanced Ice-Recrystallization Inhibition. "Splat" assays were performed using serial dilutions of both the type III multimer and the *Sf*IBP multimer (Figure 6). Images of the ice grains formed during overnight incubation were then compared to those generated in the presence of the corresponding monomeric forms of the AFPs. The concentrations of AFP multimers were compared on a "per-particle" molar basis, which has been used previously for this assay.[25] The type III multimer and monomeric type III AFP were analyzed at concentrations ranging from 1.4 to 1400 nM using 10-fold dilutions (Figure 6A). At the highest AFP monomer concentration tested (1400 nM), individual ice grains could not be distinguished, while the recrystallization inhibition activity was lost at 140 nM and in all subsequent dilutions of the protein. This result was indicated by clearly distinguishable ice grains that increased in size with each dilution of the AFP. When the same concentrations of the type III multimer were analyzed, individual ice grains were not distinguishable until a concentration of 14 nM was reached, indicating that the multimer exhibits an at least 10-fold increase in IRI activity. In fact, the crystal grain size at 1.4 nM multimer was closest in size to that of the 140 nM monomer sample, suggesting that the IRI activity of the multimer was between 10- and 100-fold better than that of the monomer.

The *Sf*IBP multimer and the corresponding monomeric protein were initially analyzed over a wide concentration range of 0.01−100 nM, using 10-fold dilutions of the protein (not shown). Once an approximate activity end point was measured, additional splat assays were performed in the concentration range from 0.23 to 3.6 nM using 2-fold dilutions of the protein (Figure 6B). When *Sf*IBP was analyzed, individual ice grains could be distinguished at 1.8 nM, with ice grains increasing in size in all subsequent dilutions. Ice grains could be distinguished for the *Sf*IBP multimer only at a concentration of 0.45 nM, indicating that the multimer has a 4-fold increase in IRI activity.

DISCUSSION

Substantial progress has been made in the design of novel protein assemblies over the past 15 years.[30] One recent advance in this area has been the use of the RosettaDesign software to computationally design novel interaction interfaces on the surface of existing oligomers to drive their self-assembly. This

DOI: 10.1021/acs.biochem.6b00864
Biochemistry 2016, 55, 6811−6820

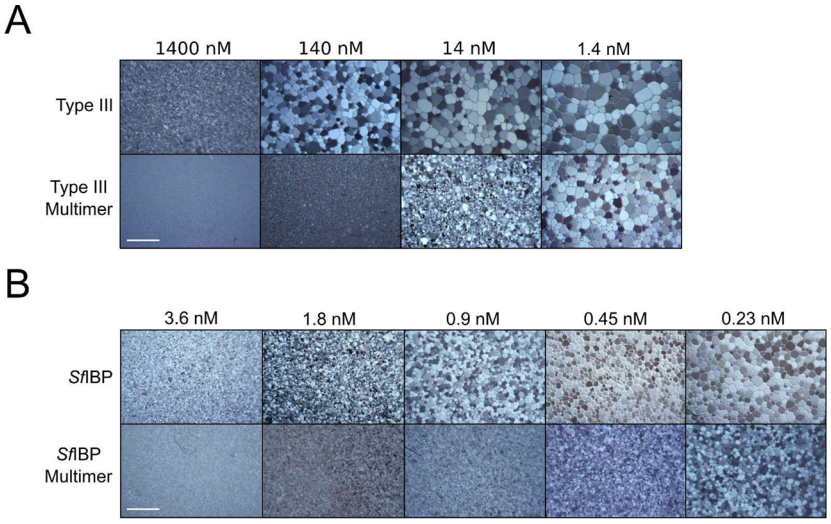

Figure 6. Effects of AFP multimerization on ice-recrystallization inhibition activity. Splat cooling assays were used to evaluate the IRI activity of AFP multimers compared to their monomeric counterparts at various concentrations. (A) The type III AFP multimer and monomeric type III AFP were measured using 1:10 dilutions over a concentration range of 1.4−1400 nM. (B) The *Sf*IBP multimer and monomeric *Sf*IBP were measured using 1:2 dilutions over a concentration range of 0.23−3.6 nM. White scale bars represent a distance of 1 mm.

was first accomplished for assemblies containing one subunit type[34] and was then extended to two-component assemblies with greater control over the assembly of subunits.[35] Several potential applications of these self-assembling protein cages have been proposed, including drug delivery, vaccine design, and custom-designed molecular machines.[34,35] Here we present an application of these protein cages for use in biotechnology, by exploiting their characteristic self-assembly to generate multimeric antifreeze protein nanomaterials.

The strategy of genetically fusing monomeric proteins to protein cages has frequently been employed in the past using natural protein assemblies.[29,49] Our work with T33-21 has further demonstrated the benefits of fusing monomeric proteins to the surface of protein cages to enhance ligand binding, in this case to ice. By genetically fusing AFPs to one component of this assembly, we have generated a homogeneous set of AFP multimers, each bearing 12 AFPs on its surface, whereas bioconjugation of type III AFP to the PAMAM dendrimers resulted in a heterogeneous mixture with incomplete occupancy of surface attachment points.[25]

We attribute the several-fold increase in TH activity of both AFP cages to the combined effects of increasing the size of the ice-binding particle and the number of AFPs that can simultaneously engage with the ice surface.[13] The latter component of the TH increase could result from improved binding to ice. Having additional ice-binding sites available to simultaneously engage ice is a way to increase the number of anchored clathrate waters available for this binding mechanism.[7] It will be interesting to determine the extent to which TH can be increased by increasing the size of the cage and the surface AFP density. To date, a multimerization strategy of assembling more than two AFP subunits together has not been seen in nature, although many natural AFPs seem to benefit from having longer isoforms (including chains of AFP domains) mixed with shorter ones.[13,21,50−53] It is possible that lower diffusion rates and tissue permeability issues work against larger constructs in a natural setting.

It could be argued that the same properties that enhance TH are at work to increase the IRI efficiency. However, we have previously suggested that AFP multimers might have an additional effect on multicrystalline ice by spanning the interstitial space to simultaneously bind and stabilize neighboring ice crystals.[25] Having AFP moieties pointing in many directions could facilitate these linkages. Also, it should be noted that ice recrystallization proceeds because large ice crystals grow at the expense of smaller ones. In addition to preventing water from joining a crystal (freezing point depression), AFPs also inhibit water from leaving an ice crystal (melting hysteresis).[54] Thus, AFP multimers bridging two ice crystals might simultaneously prevent the larger one from growing and the smaller one from shrinking.

Ice crystals in the presence of the type III multimer burst normal to the *c*-axis of the crystal (Figure 4E), while those bound by monomeric type III AFP burst parallel to this axis.[46] FIPA analysis showed that the multimer does not bind to the basal plane. Therefore, this behavior might reflect screening of the crystal tips by the large multimers binding near the apices of the hexagonal ice bipyramids, rather than binding to the basal plane at the tips. A similar effect was seen in microfluidic experiments when type III AFP-bound ice crystals turned within the chamber so that their tips were in direct contact with the polydimethylsiloxane (PDMS) surfaces and were unable to add water to the basal plane. In this situation, the crystal also "bursts" along the *a*-axes.[55] The type III multimer also exhibited a different binding pattern on the ice hemisphere during FIPA analysis compared to that of the monomer. The fluorescently labeled type III multimer was strongly bound to the periphery of the ice hemisphere but appeared to leave the pyramidal planes unbound. When type III AFP was analyzed using FIPA, it bound to both the primary prism and pyramidal planes of ice and left only the basal plane (perpendicular to the *c*-axis) unbound.[44] Type III AFP has a compound ice-binding site with one part binding to the primary prism plane of ice and the adjacent section on a slightly different AFP surface that binds the pyramidal plane. This discrepancy in the FIPA patterns might point to a restriction in the planes of ice that type III AFP is able to bind as a multimer compared to the monomer. Thus, the pyramidal ice-binding surface might be somewhat occluded in the multimer.

DOI: 10.1021/acs.biochem.6b00864
Biochemistry 2016, 55, 6811−6820

It was also interesting to note that, while the oligomerization of type III AFP led to a 10−100-fold increase in IRI activity, an only 4-fold increase was observed for that of *Sf*IBP (Figure 6). This discrepancy may be due to a suboptimal orientation of the IBS for *Sf*IBP relative to the protein cage to which it was genetically fused. The N-terminus of type III AFP is on the opposite side of the protein from its IBS and extends normal to the IBS surface.[40] Conversely, the Phyre2 model of *Sf*IBP shows that its N-terminus projects parallel to the IBS, possibly making the IBS orientation on the surface of T33-21 suboptimal for binding ice. Here it might be helpful to have a crystal or SAXS structure for the *Sf*IBP to assess this situation. A crystal structure has been determined for the T33-21 cage alone.[35] In the absence of this information, it may be necessary to explore different fusion protein linkers, such as flexible linkers, that might allow the IBS to swing outward and more effectively bind to the surface of ice.

By analyzing the type III and *Sf*IBP multimers using SDS−PAGE, we showed that each B subunit of the purified AFP multimers was connected to an AFP. Because of the design of T33-21, this means that 12 of the 24 subunits were bound to an AFP. It might be possible to attach an AFP to each of the A subunits, too, if steric clashes are not a problem. This would connect 24 AFPs on the surface of this assembly to attain even greater levels of TH and IRI activity for the AFP multimers. Having two distinct C-termini would also introduce the possibility of genetically fusing two different AFPs to the subunits of T33-21. Combinations of different AFPs, such as those that are moderately active with those that are hyperactive, could be incorporated into the same assembly in a defined stoichiometry.

■ CONCLUSIONS

In summary, computationally designed self-assembling protein cages have proven to be a viable scaffold for the oligomerization of monomeric proteins. Using two different AFPs, we showed that multimerization using this strategy generated homogeneous AFP multimers of two different types. Furthermore, we found that oligomerization in this fashion led to an increase in TH and IRI activity relative to the same concentration of the corresponding AFP monomers. New protein assemblies are continuously being designed, and we plan to explore these as potential scaffolds for IBP oligomerization. Furthermore, we envision that additional proteins may also benefit from this technology, in the event that binding to their substrate is a diffusion-controlled reaction. The fusion of these proteins to designed protein cages could lead to additional applications in biotechnology and nanoscience as well as in other fields.

■ ASSOCIATED CONTENT

Supporting Information

The Supporting Information is available free of charge on the ACS Publications website at DOI: 10.1021/acs.biochem.6b00864.

A graphic outlining the cloning strategy for the genetic fusion of AFPs to T33-21B subunits and a table of the sequences of all constructs used in this work (PDF)

■ AUTHOR INFORMATION

Corresponding Author

*E-mail: daviesp@queensu.ca. Phone: 613-533-2983.

Author Contributions

P.L.D. and S.W.P. planned the experimental methodology of the project. C.A.S. assisted with modeling AFP multimers and with TH measurements. T.D.R.V. performed initial construct design for *Sf*IBP and analyzed the TH and ice plane affinity of monomeric *Sf*IBP. N.P.K. and D.B. conceived the original design of T33-21, and N.P.K. performed the characterization of this construct and provided advice about the fusion with AFPs. S.W.P. wrote the manuscript with guidance from N.P.K., D.B., and P.L.D.

Funding

This work was funded by the Canadian Institutes for Health Research (Grant 106612). P.L.D. holds the Canada Research Chair in Protein Engineering. S.W.P. is supported by a Canadian Graduate Scholarship (CGS-M) awarded by the Natural Sciences and Engineering Research Council of Canada, as well as the Jellinck-Lyttle Graduate Fellowship in Biochemistry awarded by Queen's University. N.P.K. and D.B. are supported by the Bill and Melinda Gates Foundation, the Defense Advanced Research Projects Agency (Grant W911NF-14-1-0162), and the National Science Foundation (Grant CHE-1332907).

Notes

The authors declare no competing financial interest.

■ ACKNOWLEDGMENTS

The authors thank S. Gauthier for technical assistance, K. Basu for assistance with figure generation, and L. A. Graham and R. L. Campbell for advice.

■ ABBREVIATIONS

AFP, antifreeze protein; IBP, ice-binding protein; IBS, ice-binding site; TH, thermal hysteresis; PAMAM, polyamidoamine; FIPA, fluorescence-based ice plane affinity; IRI, ice-recrystallization inhibition.

■ REFERENCES

(1) Davies, P. L. (2014) Ice-Binding Proteins: A Remarkable Diversity of Structures for Stopping and Starting Ice Growth. *Trends Biochem. Sci. 39*, 548−555.

(2) Oude Vrielink, A. S., Aloi, A., Olijve, L. L. C., and Voets, I. K. (2016) Interaction of Ice Binding Proteins with Ice, Water and Ions. *Biointerphases 11*, 018906.

(3) Duman, J. G. (2001) Antifreeze and Ice Nucleator Proteins in Terrestrial Arthropods. *Annu. Rev. Physiol. 63*, 327−357.

(4) Graham, L. A., Hobbs, R. S., Fletcher, G. L., and Davies, P. L. (2013) Helical Antifreeze Proteins Have Independently Evolved in Fishes on Four Occasions. *PLoS One 8*, e81285.

(5) Nutt, D. R., and Smith, J. C. (2008) Dual Function of the Hydration Layer around an Antifreeze Protein Revealed by Atomistic Molecular Dynamics Simulations. *J. Am. Chem. Soc. 130*, 13066−13073.

(6) Gallagher, K. R., and Sharp, K. A. (2003) Analysis of Thermal Hysteresis Protein Hydration Using the Random Network Model. *Biophys. Chem. 105*, 195−209.

(7) Garnham, C. P., Campbell, R. L., and Davies, P. L. (2011) Anchored Clathrate Waters Bind Antifreeze Proteins to Ice. *Proc. Natl. Acad. Sci. U. S. A. 108*, 7363−7367.

(8) Knight, C. A. (2000) Structural Biology. Adding to the Antifreeze Agenda. *Nature 406*, 249−251.

(9) Kuiper, M. J., Morton, C. J., Abraham, S. E., and Gray-Weale, A. (2015) The Biological Function of an Insect Antifreeze Protein Simulated by Molecular Dynamics. *eLife 4*, e05142.

DOI: 10.1021/acs.biochem.6b00864
Biochemistry 2016, 55, 6811−6820

(10) Regand, A., and Goff, H. D. (2006) Ice Recrystallization Inhibition in Ice Cream as Affected by Ice Structuring Proteins from Winter Wheat Grass. *J. Dairy Sci. 89*, 49−57.
(11) Payne, S. R., and Young, O. A. (1995) Effects of Pre-Slaughter Administration of Antifreeze Proteins on Frozen Meat Quality. *Meat Sci. 41*, 147−155.
(12) Lee, J. R., Youm, H. W., Lee, H. J., Jee, B. C., Suh, C. S., and Kim, S. H. (2015) Effect of Antifreeze Protein on Mouse Ovarian Tissue Cryopreservation and Transplantation. *Yonsei Med. J. 56*, 778−784.
(13) Bar Dolev, M., Braslavsky, I., and Davies, P. L. (2016) Ice-Binding Proteins and Their Function. *Annu. Rev. Biochem. 85*, 515−542.
(14) Raymond, J. A., and DeVries, A. L. (1977) Adsorption Inhibition as a Mechanism of Freezing Resistance in Polar Fishes. *Proc. Natl. Acad. Sci. U. S. A. 74*, 2589−2593.
(15) Celik, Y., Drori, R., Pertaya-Braun, N., Altan, A., Barton, T., Bar-Dolev, M., Groisman, A., Davies, P. L., and Braslavsky, I. (2013) Microfluidic Experiments Reveal That Antifreeze Proteins Bound to Ice Crystals Suffice to Prevent Their Growth. *Proc. Natl. Acad. Sci. U. S. A. 110*, 1309−1314.
(16) Schrag, J. D., O'Grady, S. M., and DeVries, A. L. (1982) Relationship of Amino Acid Composition and Molecular Weight of Antifreeze Glycopeptides to Non-Colligative Freezing Point Depression. *Biochim. Biophys. Acta, Gen. Subj. 717*, 322−326.
(17) Wu, Y., Banoub, J., Goddard, S. V., Kao, M. H., and Fletcher, G. L. (2001) Antifreeze Glycoproteins: Relationship between Molecular Weight, Thermal Hysteresis and the Inhibition of Leakage from Liposomes during Thermotropic Phase Transition. *Comp. Biochem. Physiol., Part B: Biochem. Mol. Biol. 128*, 265−273.
(18) Leinala, E. K., Davies, P. L., Doucet, D., Tyshenko, M. G., Walker, V. K., and Jia, Z. (2002) A Beta-Helical Antifreeze Protein Isoform with Increased Activity. Structural and Functional Insights. *J. Biol. Chem. 277*, 33349−33352.
(19) Mok, Y., Lin, F., Graham, L. A., Celik, Y., Braslavsky, I., and Davies, P. L. (2010) Structural Basis for the Superior Activity of the Large Isoform of Snow Flea Antifreeze Protein. *Biochemistry 49*, 2593−2603.
(20) Marshall, C. B., Daley, M. E., Sykes, B. D., and Davies, P. L. (2004) Enhancing the Activity of a β-Helical Antifreeze Protein by the Engineered Addition of Coils. *Biochemistry 43*, 11637−11646.
(21) Wang, X., DeVries, A. L., and Cheng, C.-H. C. (1995) Antifreeze Peptide Heterogeneity in an Antarctic Eel Pout Includes an Unusually Large Major Variant Composed of Two 7 kDa Type III AFPs Linked in Tandem. *Biochim. Biophys. Acta, Protein Struct. Mol. Enzymol. 1247*, 163−172.
(22) Nishimiya, Y., Ohgiya, S., and Tsuda, S. (2003) Artificial multimers of the type III antifreeze protein. Effects on thermal hysteresis and ice crystal morphology. *J. Biol. Chem. 278*, 32307−32312.
(23) Baardsnes, J., Kuiper, M. J., and Davies, P. L. (2003) Antifreeze Protein Dimer: When Two Ice-Binding Faces Are Better than One. *J. Biol. Chem. 278*, 38942−38947.
(24) Can, Ö., and Holland, N. B. (2011) Conjugation of Type I Antifreeze Protein to Polyallylamine Increases Thermal Hysteresis Activity. *Bioconjugate Chem. 22*, 2166−2171.
(25) Stevens, C. A., Drori, R., Zalis, S., Braslavsky, I., and Davies, P. L. (2015) Dendrimer-Linked Antifreeze Proteins Have Superior Activity and Thermal Recovery. *Bioconjugate Chem. 26*, 1908−1915.
(26) Pollard, T. D. (1986) Mechanism of Actin Filament Self-Assembly and Regulation of the Process by Actin-Binding Proteins. *Biophys. J. 49*, 149−151.
(27) Nédélec, F., Surrey, T., and Karsenti (2003) E. Self-Organisation and Forces in the Microtubule Cytoskeleton. *Curr. Opin. Cell Biol. 15*, 118−124.
(28) Rong, J., Niu, Z., Lee, L. A., and Wang, Q. (2011) Self-Assembly of Viral Particles. *Curr. Opin. Colloid Interface Sci. 16*, 441−450.
(29) Jeon, J. O., Kim, S., Choi, E., Shin, K., Cha, K., So, I.-S., Kim, S.-J., Jun, E., Kim, D., Ahn, H. J., Lee, B.-H., Lee, S.-H., and Kim, I.-S. (2013) Designed Nanocage Displaying Ligand-Specific Peptide Bunches for High Affinity and Biological Activity. *ACS Nano 7*, 7462−7471.
(30) King, N. P., and Lai, Y. T. (2013) Practical Approaches to Designing Novel Protein Assemblies. *Curr. Opin. Struct. Biol. 23*, 632−638.
(31) Zhang, S. (2003) Fabrication of Novel Biomaterials through Molecular Self-Assembly. *Nat. Biotechnol. 21*, 1171−1178.
(32) Padilla, J. E., Colovos, C., and Yeates, T. O. (2001) Nanohedra: Using Symmetry to Design Self Assembling Protein Cages, Layers, Crystals, and Filaments. *Proc. Natl. Acad. Sci. U. S. A. 98*, 2217−2221.
(33) Leaver-Fay, A., Tyka, M., Lewis, S. M., Lange, O. F., Thompson, J., Jacak, R., Kaufman, K. W., Renfrew, P. D., Smith, C. A., Sheffler, W., et al. (2011) ROSETTA3: An Object-Oriented Software Suite for the Simulation and Design of Macromolecules. *Methods Enzymol. 487*, 545−574.
(34) King, N. P., Sheffler, W., Sawaya, M. R., Vollmar, B. S., Sumida, J. P., André, I., Gonen, T., Yeates, T. O., and Baker, D. (2012) Computational Design of Self-Assembling Protein Nanomaterials with Atomic Level Accuracy. *Science 336*, 1171−1174.
(35) King, N. P., Bale, J. B., Sheffler, W., McNamara, D. E., Gonen, S., Gonen, T., Yeates, T. O., and Baker, D. (2014) Accurate Design of Co-Assembling Multi-Component Protein Nanomaterials. *Nature 510*, 103−108.
(36) Gonen, S., DiMaio, F., Gonen, T., and Baker, D. (2015) Design of Ordered Two-Dimensional Arrays Mediated by Noncovalent Protein-Protein Interfaces. *Science 348*, 1365−1368.
(37) Jia, Z., DeLuca, C. I., Chao, H., and Davies, P. L. (1996) Structural Basis for the Binding of a Globular Antifreeze Protein to Ice. *Nature 384*, 285−288.
(38) *The PyMOL Molecular Graphics System*, version 1.7.4.3, Schrödinger, LLC, Portland, OR.
(39) Chao, H., Davies, P. L., Sykes, B. D., and Sönnichsen, F. D. (1993) Use of Proline Mutants to Help Solve the NMR Solution Structure of Type III Antifreeze Protein. *Protein Sci. 2*, 1411−1428.
(40) Antson, A. A., Smith, D. J., Roper, D. I., Lewis, S., Caves, L. S. D., Verma, C. S., Buckley, S. L., Lillford, P. J., and Hubbard, R. E. (2001) Understanding the Mechanism of Ice Binding by Type III Antifreeze Proteins. *J. Mol. Biol. 305*, 875−889.
(41) Kelley, L. A., Mezulis, S., Yates, C. M., Wass, M. N., and Sternberg, M. J. (2015) The Phyre2 Web Portal for Protein Modeling, Prediction and Analysis. *Nat. Protoc. 10*, 845−858.
(42) Garnham, C. P., Gilbert, J. A., Hartman, C. P., Campbell, R. L., Laybourn-Parry, J., and Davies, P. L. (2008) A Ca2+-Dependent Bacterial Antifreeze Protein Domain Has a Novel β-Helical Ice-Binding Fold. *Biochem. J. 411*, 171−180.
(43) Braslavsky, I., and Drori, R. (2013) LabVIEW-Operated Novel Nanoliter Osmometer for Ice Binding Protein Investigations. *J. Visualized Exp. 72*, e4189.
(44) Basu, K., Garnham, C. P., Nishimiya, Y., Tsuda, S., Braslavsky, I., and Davies, P. L. (2014) Determining the Ice-Binding Planes of Antifreeze Proteins by Fluorescence-Based Ice Plane Affinity. *J. Visualized Exp. 83*, e51185.
(45) DeLuca, C. I., Comley, R., and Davies, P. L. (1998) Antifreeze Proteins Bind Independently to Ice. *Biophys. J. 74*, 1502−1508.
(46) Scotter, A. J., Marshall, C. B., Graham, L. A., Gilbert, J. A., Garnham, C. P., and Davies, P. L. (2006) The Basis for Hyperactivity of Antifreeze Proteins. *Cryobiology 53*, 229−239.
(47) Bar-Dolev, M., Celik, Y., Wettlaufer, J. S., Davies, P. L., and Braslavsky, I. (2012) New Insights into Ice Growth and Melting Modifications by Antifreeze Proteins. *J. R. Soc., Interface 9*, 3249−3259.
(48) Garnham, C. P., Natarajan, A., Middleton, A. J., Kuiper, M. J., Braslavsky, I., and Davies, P. L. (2010) Compound Ice-Binding Site of an Antifreeze Protein Revealed by Mutagenesis and Fluorescent Tagging. *Biochemistry 49*, 9063−9071.
(49) Uchida, M., Klem, M. T., Allen, M., Suci, P., Flenniken, M., Gillitzer, E., Varpness, Z., Liepold, L. O., Young, M., and Douglas, T. (2007) Biological Containers: Protein Cages as Multifunctional Nanoplatforms. *Adv. Mater. 19*, 1025−1042.

DOI: 10.1021/acs.biochem.6b00864
Biochemistry 2016, 55, 6811−6820

(50) Kelley, J. L., Aagaard, J. E., MacCoss, M. J., and Swanson, W. J. (2010) Functional diversification and evolution of antifreeze proteins in the antarctic fish *Lycodichthys dearborni*. *J. Mol. Evol. 71*, 111−118.
(51) Wang, X., DeVries, A. L., and Cheng, C. H. (1995) Genomic basis for antifreeze peptide heterogeneity and abundance in an Antarctic eel pout: gene structures and organization. *Mol. Mar. Biol. Biotechnol. 4*, 135−147.
(52) Yu, J., Cheng, C. H., DeVries, A. L., and Chen, L. B. (2005) [Characterization of a multimer type III antifreeze protein gene from the Antarctic eel pout (*Lycodichthys dearborni*)]. *Yi Chuan Xue Bao 32*, 789−794 (Chinese).
(53) Deng, C., Cheng, C. H., Ye, H., He, X., and Chen, L. (2010) Evolution of an antifreeze protein by neofunctionalization under escape from adaptive conflict. *Proc. Natl. Acad. Sci. U. S. A. 107*, 21593−21598.
(54) Celik, Y., Graham, L. A., Mok, Y.-F., Bar, M., Davies, P. L., and Braslavsky, I. (2010) Superheating of Ice Crystals in Antifreeze Protein Solutions. *Proc. Natl. Acad. Sci. U. S. A. 107*, 5423−5428.
(55) Drori, R., Davies, P. L., and Braslavsky, I. (2015) When Are Antifreeze Proteins in Solution Essential for Ice Growth Inhibition? *Langmuir 31*, 5805−5811.

DOI: 10.1021/acs.biochem.6b00864
Biochemistry 2016, 55, 6811−6820